ELSEVIER

Journal of Magnetism and Magnetic Materials 152 (1996) 61–69

Journal of magnetism and magnetic materials

Structural and magnetic properties of barium hexaferrite nanostructured particles prepared by the combustion method

S. Castro [a], M. Gayoso [a], J. Rivas [b,*], J.M. Greneche [c], J. Mira [b], C Rodríguez [a]

[a] *Department of Inorganic Chemistry, University of Santiago de Compostela, E-15706 Santiago de Compostela, Spain*
[b] *Department of Applied Physics, University of Santiago de Compostela, E-15706 Santiago de Compostela, Spain*
[c] *Department of Materials Physics, URA-CNRS 807, University of Maine, F-72017 Le Mans, France*

Received 21 March 1995; revised 8 June 1995

Abstract

The combustion method, a fast and simple way of preparing sub-micrometer sized particles from a solution of the corresponding metal nitrates and a reducing agent (ODH, TFTA) which is used as a fuel, was adapted to the synthesis of barium hexaferrite particles. Structural and magnetic properties were investigated by X-ray diffraction, transmission electronic microscopy, magnetic measurements and Mössbauer spectrometry on nanostructured as well as on microstructured particles resulting from annealing treatments under different conditions. High values of the coercive field (5.3 kOe) and of the magnetization (57.8 emu/g), at 13.5 kOe, were obtained on well crystallized $BaFe_{12}O_{19}$ particles annealed at 850°C.

1. Introduction

Hexagonal magnetic hard ferrites such as $BaFe_{12}O_{19}$ are currently magnetic materials with great scientific and technological interest, because of their relatively strong anisotropy and moderated, but still interesting magnetization. The production of barium hexaferrite permanent magnets, their application in microwave devices, or the use of hexaferrite fine particles in perpendicular magnetic recording, represent areas in which barium hexaferrite plays an important role.

In the case of fine particles (~ 0.1 μm), one can expect peculiar magnetic properties compared with those observed for sintered materials [1]. On the one hand, the value of the coercive field increases whereas the magnetic losses decrease, and on the other, the values of the saturation magnetization and coercive fields are observed to be lower than those expected for this type of particles. Sometimes this behaviour can be explained through surface effects [2–4], particle size and morphology [3,5,6], impurities [7], or crystallographic defects [4,7,8]. In any case, the magnetic properties of these materials depend largely on the microstructure, and the microstructure depends on the preparation method. Recently, a wide range of chemical methods have been used to obtain ultrafine mixed oxide particles, all of which require a low-temperature process in order to control the growth of the particles as a first synthesis stage. Some of these methods are: the organometallic precursor method [9], the pyrosol method [4], chemical coprecipitation [7], sol–gel [10], mechanical milling [11], etc. However, a number of difficulties in obtaining particles of small and homogeneous sizes with high chemical purity as well as in a crystallized state, have been pointed out in most

* Corresponding author. Email: rivas@gaes.usc.es; fax: +34-81-520676;

0304-8853/96/$15.00
SSDI 0304-8853(95)00450-5

papers reporting the synthetic methods developed up to now.

In the present paper we report the structural and magnetic properties of $BaFe_{12}O_{19}$ nanostructured particles synthesized using the combustion method [12]. This method was successfully applied to the production of mixed oxides with spinel, garnet and orthoferrite structures [13–15] as well as high-temperature superconductors [16]. In this process, we make use of the great exothermicity of the redox reaction between metal nitrates oxidizing agents and tetraformal trisazine (TFTA, $C_4H_{12}N_6$), or oxalic acid dihydrazide (ODH, $C_2H_6N_4O_2$), reducing agents, to generate, in a short time, sub-micrometer sized particles ($\ll 0.1$ μm), which after an annealing process result in $BaFe_{12}O_{19}$ microstructured particles.

In order to study the structural and magnetic properties of these particles, we have used X-ray powder diffraction and Mössbauer spectrometry techniques which provide information on the lattice parameters, the presence of impurity phases, the different iron phases, the distribution of the iron ions in the lattices, as well as the hyperfine parameters.

2. Sample preparation

The corresponding metal nitrates and adequate quantities of reducing agents were dissolved in the minimum amount of water required for their solution. Tetraformal trisazine (TFTA, $C_4H_{12}N_6$), was prepared by means of the reaction of formaldehyde and hydrazine hydrate at 0°C [17]. The stoichiometric compositions of the reducing agent–metal nitrate mixtures were calculated taking into account the concepts of propellant chemistry [18], the equivalence ratio ϕ_e, and the reducing and oxidizing element valences. Let us remark that in this context, C, H, Ba and Fe are the reducing species with valences of +4, +1, +2 and +3, respectively, whereas O is the oxidizing species with a valence of −2; the valence of nitrogen is taken as zero.

Table 1
Reactive proportions for the preparation of $BaFe_{12}O_{19}$ sample series. All the samples were prepared from 0.405 g of $Ba(NO_3)_2$ and 7.500 g of $Fe(NO_3)_3 \cdot 9H_2O$. ϕ_e is the equivalence ratio

Sample	Amount of reducing agent (g)	Molar proportion nitrates: reducing agent	ϕ_e
ODH			
A	3.466	1:1.46	1
B	6.932	1:2.92	0.68
C	6.932	1:2.92	0.68
TFTAZ			
X	1.544	1:0.52	1
Y	3.088	1:1.05	0.55
Z	3.088	1:1.05	0.55

Table 2
Thermal treatment conditions applied to $BaFe_{12}O_{19}$ samples. Note that all the ash samples were first heated at 350°C for 1 h

Sample	Thermal treatment
X1, Y1, A1, B1	700°C/100 h
A2, B2	700°C/4 h + 750°C/100 h
X3, Y3, A3, B3	700°C/4 h + 1000°C/4 h
C1, Z1	700°C/100 h
C2, Z2	700°C/100 h + 750°C/100 h
C3, Z3	700°C/100 h + 750°C/100 h + 850°C/100 h
C4, Z4	700°C/100 h + 1000°C/100 h

Series of samples were prepared with each reducing agent. The proportion of reducing agent was varied along each series in order to check its influence on the size and purity of the particles. The ratio of metal nitrates to ODH (or TFTA) reducing agent was: $Ba(NO_3)_2$:$Fe(NO_3)_3 \cdot 9H_2O$: ODH (TFTA) = 1:12:19 (6.8) and 1:12:38 (13.6) and the quantities used are shown in Table 1.

The mixture containing the metal nitrates and the reducing agent was heated to boiling with frothing and foaming. At the point of complete dehydration, the foam ignites (sometimes it even flames) at a temperature of approximately 300°C for 5 min or less. The combustion residue is ash-like, foamy and brown. It is concluded that the porosity of the ash increases with the quantity of reducing agent, whereas the density decreases. After burning, the ash was annealed at temperatures of 700–1000°C to obtain barium hexaferrite particles. The results obtained on the samples are presented in Table 2. They correspond to ash samples annealed at 700, 750, 850 and 1000°C for 100 h in cumulative or independent treatments.

The combustion method has the advantage of permitting the production of barium hexaferrite precursor materials in a quick and simple manner, without any special setup or complicated chemical reac-

tions, in contrast with some of the other methods mentioned above.

3. Experimental results

The samples were characterized by X-ray powder diffraction on a Philips PW1710 diffractometer using Cu Kα radiation. All patterns were taken at room temperature, in the step-scan mode spanning an angular range of 110° in 2θ (from 10° to 120°) in steps of 0.04° 2θ, and a counting time of 16–29 s per step. The sizes and shapes of the particles were analyzed by transmission electron microscopy (TEM) on a Philips CM12 microscope operated at 100 kV.

^{57}Fe absorption Mössbauer spectroscopy was carried out using a conventional spectrometer operating in the constant acceleration mode and a ^{57}Co source diffused in a Rh matrix. Previous Mössbauer studies on crystalline $BaFe_{12}O_{19}$ have revealed rather complex spectra, because the hyperfine structure results from the presence of five kinds of iron sites. As the highest resolution is observed at room temperature, the Mössbauer spectra were systematically performed on all the samples at room temperature. The hyperfine data were refined with the Mosfit program. The values of the chemical isomer shift are reported relative to metallic α-Fe at room temperature.

The magnetic properties were measured with a vibrating sample magnetometer VSM operating in magnetic fields between $0 \leq H \leq 13.5$ kOe in the temperature range 77 K $\leq T \leq$ 1100 K.

3.1. X-ray and TEM results

The ash resulting from the combustion, which was studied by X-ray diffraction, is a mixture of iron oxides and barium nitrate particles. Broad Bragg peaks were evidenced and the broadening was attributed to the small particle size and to the lack of crystallinity of the samples. When the ash is annealed at 700°C for 2 h, an important amount of $BaFe_{12}O_{19}$ phase occurs: the presence of very well-defined Bragg peaks indicates a good crystalline state of the samples (Fig. 1). We then performed a Rietveld refinement [19] of the X-ray powder diffraction patterns of the samples using the Fullprof [20] and ARIT4 [21] programs. This refinement using the $P6_3/mmc$ space group confirms the well established hexagonal phase of $BaFe_{12}O_{19}$ (Fig. 2). The lattice parameters, which are in good agreement with the more common published data [22], remain indepen-

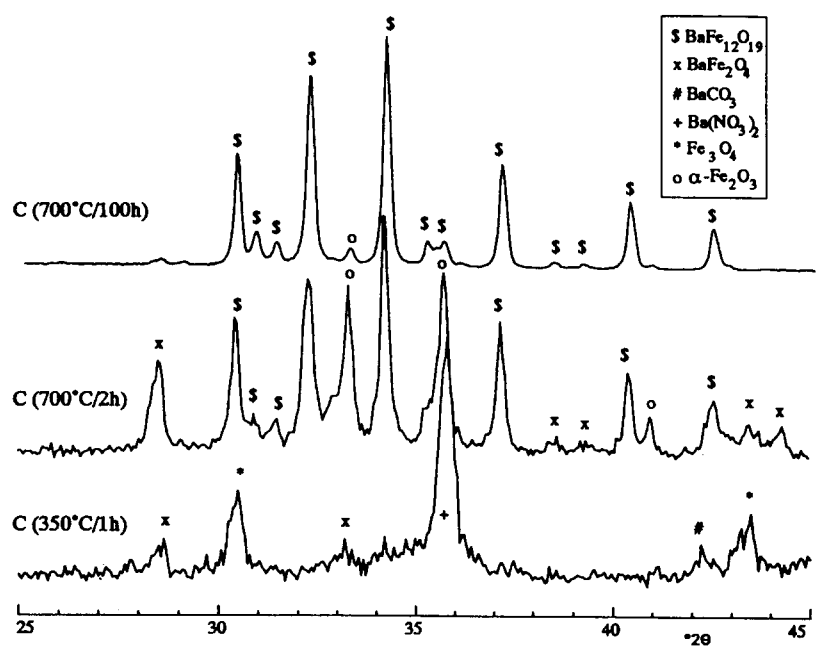

Fig. 1. X-ray diffractograms of sample C after different thermal treatments.

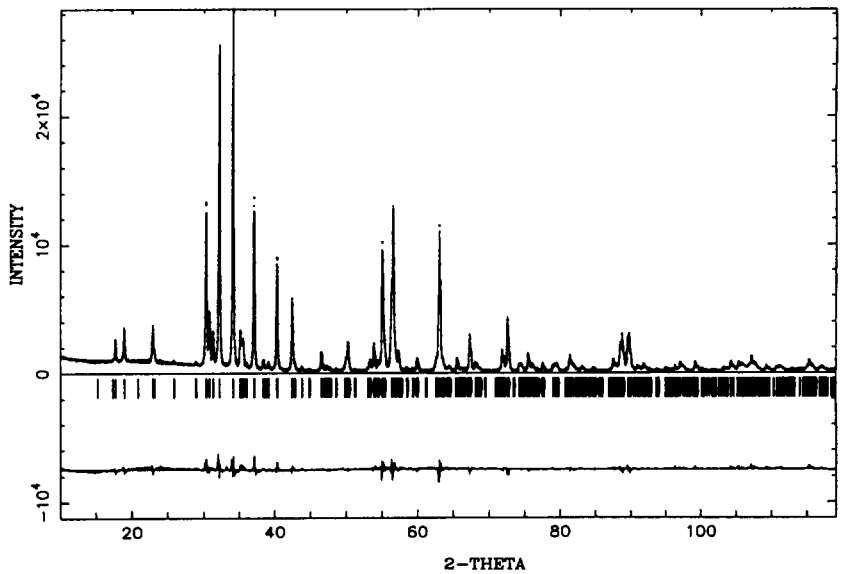

Fig. 2. X-ray diffractogram of sample C3 and Rietveld refinement results.

dent of the annealing treatment of the samples. Also, for the as-prepared sample, we note the presence of two additional compounds, identified as hematite α-Fe_2O_3 and barium monoferrite $BaFe_2O_4$ phase impurities induced during the synthesis. These impurities represent less than 10% in all the samples, except for the sample prepared with the smallest amount of reducing agent (X1), which has 50% of these impurities. After annealing at 750°C, the minor phase was reduced to less than 5% in all samples, and after annealing at 850°C it was reduced to less than 1%.

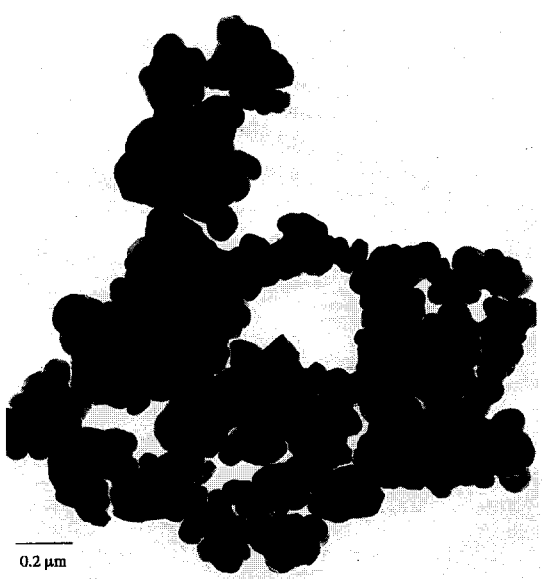

Fig. 3. TEM micrographs of sample C3.

The electron transmission micrographs in Fig. 3 (sample C3) clearly show nanostructured particles for the low-temperature annealed samples (the average diameter is estimated at 70 nm). The size of the particles increases slightly with annealing temperature: for treatments at 750, 850 and 1000°C, the average diameters are 0.1, 0.3 and 0.5 μm, respectively (see Table 3).

The as-prepared particles are agglomerated due to sintering. They are platelet-shaped, more spherical for low annealing temperatures and with a tendency towards a hexagonal shape for higher annealing temperatures.

3.2. Magnetic results and discussion

The Mössbauer spectra (see Fig. 4) were fitted assuming the presence of five iron components (12k, $4f_1$, $4f_2$, 2a and 2b), in agreement with the assignment proposed by Evans et al. [23]. Two additive components corresponding to α-Fe_2O_3, hematite, and $BaFe_2O_4$, barium monoferrite, were also introduced during the fitting procedure. The contribution of the

hematite phase is not easy to estimate because the values of its hyperfine parameters are very close to those of the $4f_2$ iron site.

Due to small discrepancies in the relative population of iron in the 12k position, regardless of the sample and of the annealing treatment conditions, we assumed the theoretical value of the population in all samples to be 50% of the amount of iron in $BaFe_{12}O_{19}$. According to this assumption, we have estimated the relative populations of the other barium hexaferrite iron positions. The differences between the refined and the calculated values of the relative population of $4f_2$ position have been attributed to the presence of Fe^{3+} corresponding to the α-Fe_2O_3 phase, due to the similarity of the hyperfine parameters. Thus we have obtained an estimate of the proportion of α-Fe_2O_3 that agrees quite well with the results provided by X-ray diffraction. The second impurity, $BaFe_2O_4$, was not observed (the weight in iron atoms was estimated at less than 0.5%).

The final values of the hyperfine parameters, except for those of the quadrupole shift, were very similar to those obtained on well-characterized and well-crystallized $BaFe_{12}O_{19}$ samples (prepared from high-purity initial materials) obtained after longer annealing (see Table 4).

The fluctuations observed in the isomer shift and hyperfine field values, corresponding to the 2b iron positions, are explained by the rather small contribution of this position; however, in the cases of the positions with larger populations ($4f_1$ and 12k), the final values of the hyperfine parameters are very similar to those obtained on well-characterized and

Table 3
Impurities, size and magnetic data for $BaFe_{12}O_{19}$ particles. H_c and M_s were measured at room temperature, for H_{max} = 13.5 kOe. % is the percentage, by weight, of impurities obtained from X-ray diffraction. D is the average diameter of the particles obtained from TEM. μ_B is the number of Bohr magnetons obtained from Mössbauer spectrometry

Sample	Annealing temperature (°C)	$BaFe_2O_4$ (%)	α-Fe_2O_3 (%)	D (μm)	H_c (Oe)	M_s (emu/g)	μ_B
C1	700	0	2.5	< 0.1	5208	54.3	25
C2	750	0	1.4	0.05–0.15	5256	55.7	27
C3	850	0	0	0.15–0.20	5285	57.8	29
C4	1000	0	0	0.15–0.50	5145	59.0	34
Z1	700	3.8	13.0	< 0.1	4709	46.8	31
Z2	750	2.1	7.9	0.05–0.15	4800	51.0	32
Z3	850	0	1.6	0.15–0.20	4893	55.6	35
Z4	1000	0	0	0.15–0.50	4597	57.4	35
A1	700	5.4	1.2	< 0.1	5379	52.8	28.7
A2	750	5.2	1.6	–	–	–	–
A3	1000	0	0	0.2–0.5	5209	58.0	29.4
B1	700	5.0	1.1	< 0.1	4792	47.7	22.6
B2	750	3.3	0.7	–	–	–	–
B3	1000	0	0	0.2–0.5	4895	52.6	38.2
X1	700	25.2	10.4	< 0.1	4192	29.8	13
X3	1000	0	0	0.1–0.3	3980	55.5	22.6
Y1	700	3.5	0.4	< 0.1	4692	48.6	42.4
Y3	1000	0	0	0.1–0.5	4679	55.4	40.3
Sintered ceramic	1100	0	0	> 2	1925	57.5	29

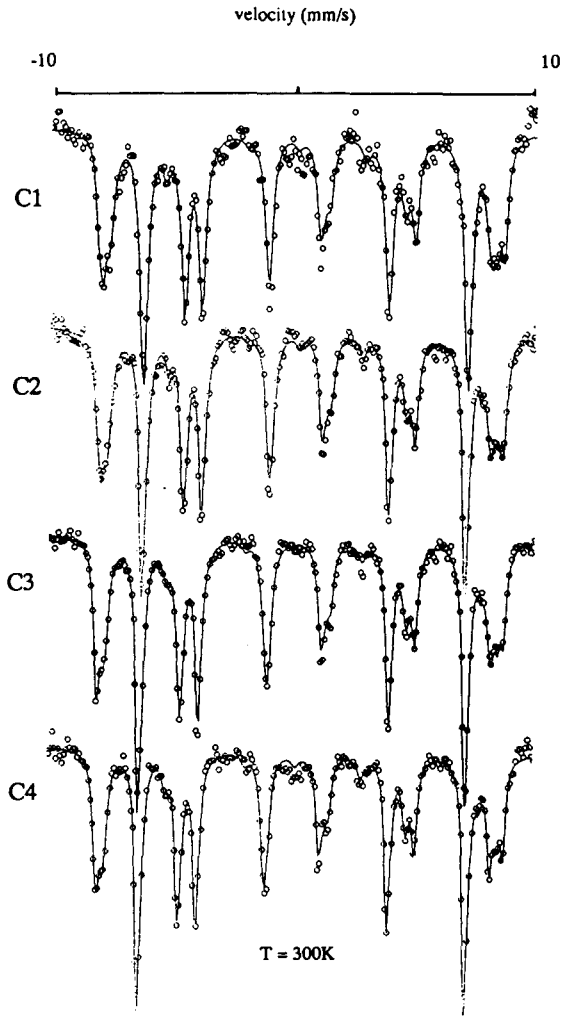

Fig. 4. Mössbauer spectra of samples C1, C2, C3 and C4.

well-crystallized $BaFe_{12}O_{19}$ samples synthesized according to the usual ceramic method.

In addition, a small discrepancy in the relative populations for the iron sites can be observed as compared to the expected values: the relative population for the $4f_1$ and 2a positions is higher than expected, in contrast with the case of the 2b and 12k positions.

First, the relatively large population of the $4f_1$ position, and secondly, the small populations of the 2b and 12k positions, whose spins are aligned antiparallel and parallel, respectively, to the resulting direction of the magnetization, lead to a lowering of the number of the Bohr magnetons, μ_B, for $BaFe_{12}O_{19}$. Even though the high population of the 2b position leads to an increase in the number of Bohr magnetons, it is not sufficient to compensate for this reduction. These features explain (i) the discrepancy with the theoretical Bohr magnetons estimated on the well-crystallized $BaFe_{12}O_{19}$, and (ii) the increase in the number of Bohr magnetons for the better crystallized samples, resulting from either larger annealing times or higher annealing temperatures.

Hysteresis loops were recorded between $-13.5 \leq H \leq 13.5$ kOe for the different samples and at different temperatures (see Fig. 5), and the corresponding values of the coercive field, H_c, and the magnetization, M_s, for 13.5 kOe are given in Table 3 and Fig. 6.

The increase in the magnetization with annealing temperature is attributed to the improved purity and crystallinity of the $BaFe_{12}O_{19}$ phase, as defined by X-ray diffraction and Mössbauer spectrometry. The presence of small quantities of α-Fe_2O_3, which is a weak ferromagnet at temperatures below $T_N = 634$°C, or of $BaFe_2O_4$, which is antiferromagnetic at temperatures below $T_N = 607$°C, in the hexaferrite samples annealed at low temperatures, gives a slightly reduced magnetization of the samples compared with the magnetization values for the samples without this impurity (Table 3).

Furthermore, the relative populations of the different iron positions, which determine μ_B, will also

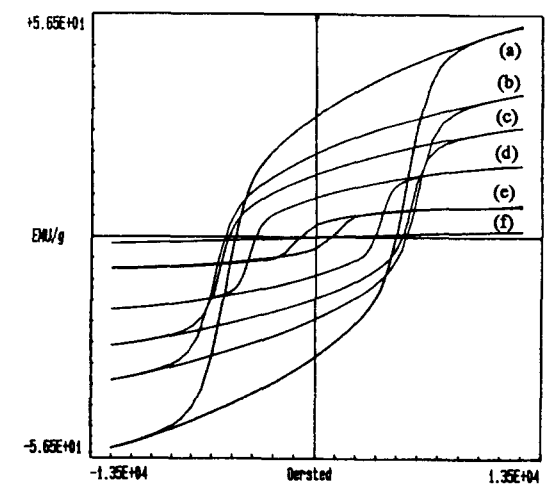

Fig. 5. Hysteresis loops of sample C3 at temperatures T = (a) 20, (b) 200, (c) 300, (d) 400, (e) 450 and (f) 500°C.

Table 4
Hyperfine parameters at the different iron sites for $BaFe_{12}O_{19}$ samples: isomer shift IS (mm/s) given relative to metallic iron at 300 K, quadrupole shift 2ε (mm/s), hyperfine field H_{hf} (T) and relative area (%) of the subspectra

Position	12k				$4f_1$				$4f_2$				2a				2b			
Parameter	IS	2ε	H_{hf}	%	IS	2ε	H_{hf}	%	IS	2ε	H_{hf}	%	IS	2ε	H_{hf}	%	IS	2ε	H_{hf}	%
Error	±01	±01	±4	±2	±01	±01	±4	±2	±01	±02	±4	±3	±01	±05	±4	±2	±01	±05	±4	±2
C1	0.35	0.40	41.5	50.3	0.27	0.26	48.9	21.0	0.43	0.11	51.3	16.3	0.27	−0.02	51.0	5.9	0.34	2.20	41.2	6.5
C2	0.36	0.40	41.4	50.8	0.26	0.18	48.9	18.3	0.40	0.15	51.3	18.1	0.29	−0.03	51.1	7.9	0.28	2.21	40.2	4.9
C3	0.36	0.39	41.4	50.2	0.26	0.20	49.0	20.9	0.40	0.16	51.5	14.6	0.32	0.03	50.9	9.3	0.28	2.24	40.0	5.0
C4	0.37	0.40	41.5	49.2	0.27	0.20	49.1	19.7	0.40	0.23	51.5	13.0	0.34	−0.04	51.1	11.2	0.30	2.16	39.7	6.9
Z1	0.36	0.40	41.5	43.1	0.28	0.19	48.8	20.7	0.47	0.01	51.4	13.7	0.29	−0.07	51.4	18.5	0.30	2.17	39.8	4.0
Z2	0.35	0.40	41.4	46.1	0.28	0.20	48.8	20.5	0.47	0.07	51.4	13.3	0.29	−0.01	51.3	15.8	0.28	2.19	40.0	4.2
Z3	0.35	0.40	41.5	49.7	0.26	0.22	49.0	19.1	0.41	0.15	51.4	13.1	0.31	0.01	51.2	13.1	0.30	2.21	40.3	5.1
Z4	0.36	0.40	41.4	50.8	0.27	0.21	48.9	18.2	0.41	0.20	51.5	14.4	0.32	0.01	51.0	12.0	0.27	2.27	39.9	4.5
Sintered ceramic	0.35	0.40	41.4	50.4	0.27	0.21	48.9	16.1	0.39	0.19	51.4	19.4	0.31	−0.02	50.6	8.9	0.30	2.20	40.0	5.2
% theor.				50.0				16.7				16.7				8.3				8.3

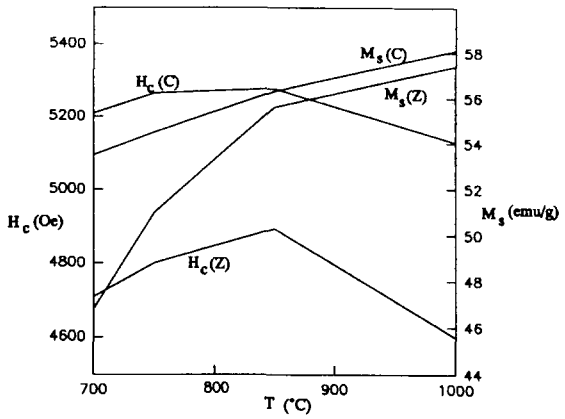

Fig. 6. Evolution of M_s and H_c with thermal treatment of samples C and Z.

determine the resulting magnetization for each sample. If we take a series of samples annealed at different temperatures we can observe how the sign of the variation of the resultant magnetization agrees with that of the variation of μ_B calculated from Mössbauer spectrometry. Increased annealing time and temperature gives an increase in the magnetization, which leads to an increase of μ_B. This is because an increased diffusion of Fe^{3+} ions in the lattice is favoured, and the relative population values approach the theoretical ones corresponding to pure barium hexaferrite. This explains why the magnetization values of the small particles are smaller than expected. This has been observed before [8].

The difference between the theoretical and the experimental values of the iron site populations, which is larger in the case of the samples annealed at 700 and 750°C than in those annealed at 850 and 1000°C, can be also attributed to stacking faults of the RSR*S* blocks.

At room temperature, the values of the coercive field H_c remain high, regardless of the annealing treatment conditions ($4.8 < H_c < 5.3$ kOe). These values are similar to those expected for single-domain hexaferrite particles [24], with a tendency to increase with annealing temperature up to 850°C, because the crystallinity and purity of the samples is better. However, at higher temperatures, H_c drops due to the increase in grain size, i.e. to a smaller nucleation field [25–29].

Fig. 7 shows the evolution of the magnetization M_s and that of the coercive field H_c at 13.5 kOe with temperature (between room temperature and the Curie temperature, T_C). One can observe the decreasing values of M_s when the temperature increases, up to T_C. However, H_c increases with temperature up to 200–300°C and then decreases at higher temperatures. These results can be explained by assuming a single-domain structure around 200–300°C. Kools [28,29] proposed the following expression for the coercivity:

$$H_c = a \cdot H_A - b \cdot M_s,$$

where the first term represents the average internal field needed to nucleate a reversed domain, and the second term corresponds to the effect of internal demagnetization fields. In our case, H_A is nearly independent of T (up to 300°C) and M_s decreases with T, implying a positive temperature coefficient for the coercivity, H_c.

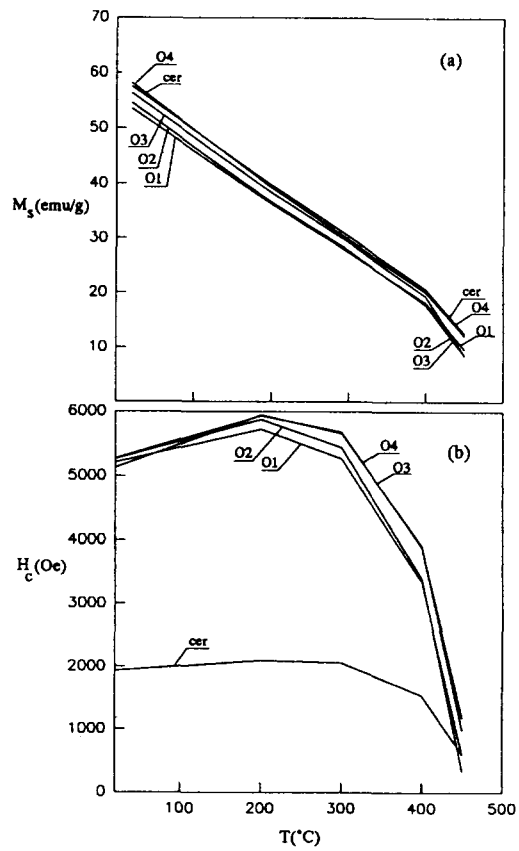

Fig. 7. Evolution of (a) M_s and (b) H_c of samples C1, C2, C3, C4 and a ceramic sample, with temperature.

4. Conclusions

The present results give clear evidence of the potential the combustion method: under optimal conditions and adequate annealing treatment, this process leads to the synthesis of barium hexaferrite nanostructured particles. Furthermore, it confirms the compromise that must be made when obtaining crystalline pure single-domain $BaFe_{12}O_{19}$ particles. The magnetic performance of the $BaFe_{12}O_{19}$ particles resulting from annealing at approximately 850°C is promising: the main magnetic characteristics (magnetization value of 57.8 emu/g and coercive fields of 5285 Oe, at 13.5 kOe), are attributed to the high purity ($< 1\%$ of impurities), good crystalline state, and the small homogeneous size of the particles (the dimensions of platelet-shaped particles are in the range 0.1–0.2 μm).

Acknowledgements

The authors would like to thank Professor J.L. Fourquet and G. Courbion for helpful discussions. One of us (S.C.) thanks the Xunta de Galicia for scholarships (1990–94) and for providing financial support for a stay at the University of Le Mans (France).

References

[1] V. Ens, in: Ferromagnetic Materials, vol. 3, ed. P. Wohlfarth (North-Holland, Amsterdam, 1982), p. 3.
[2] X. Battle, X. Obradors, M. Medarde, J. Rodríguez-Carvajal, M. Pernet and M. Vallet-Regí, J. Magn. Magn. Mater. 124 (1993) 228.
[3] K. Haneda and A.H. Morrish, IEEE Trans. Magn. 25(3) (1989) 2597.
[4] M.V. Cabañas, J.M. González-Calvet, M. Labeau, P. Mollard, M. Pernet an M. Vallet-Regí, J. Solid State Chem. 101 (1992) 265.
[5] Z.X. Tang, S. Nafis, C.M. Sorensen, G.C. Hadjipanayis and K.J. Klabunde, IEEE Trans. Magn. 25 (1989) 4236.
[6] G.C. Hadjipanayis, E. Singleton and Z.X. Tang, J. Magn. Magn. Mater. 81 (1989) 318.
[7] K. Haneda, C. Miyakawa and H. Kojima, J. Am. Ceram. Soc. 57(8) (1974) 354.
[8] V.K. Sankaranarayanan, Q.A. Pankhurst, D.P.E. Dickson and C.E. Johnson, J. Magn. Magn. Mater. 125 (1993) 199.
[9] F. Licci, G. Turilli and T. Besagni, IEEE Trans. Magn. 24 (1988) 593.
[10] E. Lucchini, S. Meriani, F. Delben and S. Paoletti, J. Mater. Sci. 19 (1984) 121.
[11] J.M. Greneche, F. Boust, E. Flaven and H. Pascard (unpublished results on $BaFe_{12}O_{19}$); for the system $SrFe_{12}O_{19}$ see, for example, U. Heinecke, C. Cruz, E. Wieser and C. Bernhardt, Phys. Stat. Solidi (a) 77 (1983) 225.
[12] S. Castro, Doctoral Thesis, Santiago de Compostela, Spain (1994).
[13] K. Suresh, N.R.S. Kumar and K.C. Patil, Adv. Mater. 3 (1991) 148.
[14] K. Suresh and K.C. Patil, J. Solid State Chem. 99 (1992) 12.
[15] S. Sundar Manoharan and K.C. Patil, J. Solid State Chem. 102 (1993) 267.
[16] S. Sundar Manoharan, V. Prasad, S.V. Subramanyan and K.C. Patil, Physica C 190 (1992) 225.
[17] E.W. Schmidt, Hydrazine and its Derivatives (Wiley, New York, 1984), p. 313.
[18] S.R. Jain, K.C. Adiga and V.R. Paiverneker, Combust. Flame 40 (1981) 71.
[19] H.M. Rietveld, Acta Crystallogr. 22 (1967) 151; H.M. Rietveld, J. Appl. Crystallogr. 2 (1969) 65.
[20] J. Rodríguez-Carvajal, Program Fullprof, Abstr. Satellite Mtg. on Powder Diffraction, XV Congr. Int. Union of Crystallography (Toulouse, 1990), p. 127.
[21] A. Le-Bail, H. Duroy and J.L. Fourquet, Mater. Res. Bull. 23 (1988) 447.
[22] X. Obradors, A. Collomb, M. Pernet, D. Samaras and J.C. Joubert, J. Solid State Chem. 56 (1985) 171.
[23] B.J. Evans, F. Granjean, A.P. Lilot, R.H. Vogel and A. Gerard, J. Magn. Magn. Mater. 67 (1987) 123.
[24] K. Haneda and A.H. Morrish, IEEE Trans. Magn. 25 (1989) 2597.
[25] J. Smith and H.P.J. Wijn, Ferrites (Philips Techn. Library, Eindhoven, 1960).
[26] H. Kojima, in: Ferromagnetic Materials, vol. 3, ed. E.P. Wohlfarth (North-Holland, Amsterdam, 1982).
[27] H. Kronmüller, in: Superparamagnets, eds. G.J. Long and F. Grandjean (Kluwer, Dordrecht, 1991), ch. 19, p. 461.
[28] F. Kools, Proc. Magnetic Materials and their Applications (MMA), Grenoble, J. Physique 46 (1985) C6-349.
[29] F. Kools and D. Stoppels, Kirk–Othmer Encyclopedia of Chemical Technology, 4th edn, vol. 10, Ferrites (Wiley, New York, 1994), p. 381.